Rock and Soil Mechanics

Volume 42 | Issue 8 Article 9

12-16-2021

Compression test and numerical simulation research on improved red beds subgrade fillers in Sichuan–Tibet Railway

Hua XU
School of Civil Engineering, Southwest Jiaotong University, Chengdu, Sichuan 610031, China

Ting-yu ZHOU
School of Civil Engineering, Southwest Jiaotong University, Chengdu, Sichuan 610031, China

Xin-yu WANG
China Railway Eryuan Engineering Group Co., Ltd., Chengdu, Sichuan 610031, China

Jie ZHANG
China Construction Third Engineering Bureau Co., Ltd., Wuhan, Hubei 430070, China

See next page for additional authors

Custom Citation

XU Hua, ZHOU Ting-yu, WANG Xin-yu, ZHANG Jie, ZHANG Xiao-bo, LIU Yu-chen, . Compression test and numerical simulation research on improved red beds subgrade fillers in Sichuan–Tibet Railway[J]. Rock and Soil Mechanics, 2021, 42(8): 2259-2268.

Compression test and numerical simulation research on improved red beds subgrade fillers in Sichuan–Tibet Railway

Authors

Hua XU, Ting-yu ZHOU, Xin-yu WANG, Jie ZHANG, Xiao-bo ZHANG, and Yu-chen LIU

Rock and Soil Mechanics 2021 42(8): 2259−2268 ISSN 1000−7598
https: //doi.org/10.16285/j.rsm.2020.6966 rocksoilmech.researchcommons.org/journal

Compression test and numerical simulation research on improved red beds subgrade fillers in Sichuan–Tibet Railway

XU Hua[1], ZHOU Ting-yu[1], WANG Xin-yu[2], ZHANG Jie[3], ZHANG Xiao-bo[1], LIU Yu-chen[1]

1. School of Civil Engineering, Southwest Jiaotong University, Chengdu, Sichuan 610031, China
2. China Railway Eryuan Engineering Group Co., Ltd., Chengdu, Sichuan 610031, China
3. China Construction Third Engineering Bureau Co., Ltd., Wuhan, Hubei 430070, China

Abstract: The red beds are widely distributed in Yunnan, Guizhou, Sichuan and Southeast Asia. This material is not suitable as subgrade filling due to seriously weathering and its softening characteristic after absorbing water. In the project of the section between Chengdu and Ya'an of Sichuan–Tibet Railway, the graded weakly weathered red-mudstone fragments was added to red beds subgrade fillers with specific proportion to improve size distribution and compactness of the material. The stress–strain characterization of improved red beds subgrade fillings has been obtained from laboratory test. A method of randomly generating fragment geometry model with concave convex polyhedron shape has been proposed. Based on the numerical compression model established by PFC^{3D}, the proportion of different strong force chains during loading and probability density distribution at the peak intensity have been studied. The results show that the improved red beds subgrade fillings with the stone content of 50% performs better mechanically with good deformation characteristics, and its unconfined compressive strength is 421.9 kPa. The fragments form super chains easily by friction under bond strength of red clay and that strengthens the system. The mechanical properties degree of improved red beds subgrade fillers follows the order of the stone content 50%> 40%> 60%. Therefore, it is recommended to add 50% of weakly weathered red-mudstone fragment as the subgrade fillings when improving the red bed clay of the Sichuan–Tibet Railway.

Keywords: Sichuan–Tibet Railway; red beds; soil–rock mixture; particle flow code (PFC); rock block shape

1 Introduction

The red beds refer to the clastic rock sedimentary stratum with red dominant color, which are widely distributed in Yunnan, Guizhou, Sichuan and Southeast Asia. Under wet and rainy climate conditions, red beds tend to soften to form special soft clay, and consequently trigger vertical settlement under the load of embankment and dynamic load of vehicles. Therefore, the red beds are not suitable to be directly used as subgrade filling[1–2]. The Chengdu–Ya'an section of the Sichuan–Tibet Railway is located in the southwest mountainous area, passing through the Sichuan Basin, with a large area of red beds distributed along the line. Due to the restriction of geological conditions and construction cost, the project adopts a physical method to improve the railway subgrade by mixing the red clay with weakly weathered mudstone rock to obtain high-quality fillers that satisfy the design requirement of railway specifications[3–4]. This method not only reduces the cost of railway construction and waste, but also effectively protects the natural environment, realizing significant economic and ecological benefits. The improved red beds subgrade fillers are special soil-rock composite materials, and there is lack of experience for its application in the construction of the red-bed area. The systematic study of the strength and failure characteristics of this material is of great significance to the construction projects under this geological condition.

Unconfined compression test takes the advantages of simple operation, fast loading and accurate results, and it is an important test method to determine the macroscopic constitutive characterization, compressive strength and failure mode of materials[5]. At present, a considerable number of scholars have carried out unconfined compression tests on the improved soil to obtain the data of strength and deformation, and then evaluate the improvement effect and investigate the optimum plan[6]. However, it is difficult to explain the substantial mechanism for stress and deformation through unconfined compression tests. In recent years, particle flow numerical simulation technology based on discrete element analysis, such as PFC (particle flow code), enables simulation of soil particles(ball) and block stone particles(clump)[7] to monitor the changes of particles, contact force chains, cracks, energy and other related physical quantities[8–9]. The micro-mechanical mechanism of rock and soil medium can be well studied and explained.

In this paper, the unconfined compression test is combined with particle flow numerical simulation to analyze the macroscopic and micro-mechanical deformation characteristics of the improved red beds subgrade fillers. The method for randomly constructing a geometric model of crushed stone with concave-convex polyhedron shape was proposed. A geometric model conforming to the filler particle gradation has been established, and the variations of different types of strong contact force chains were innovatively analyzed to explain the substantial mechanism of the factors affecting the strength of the improved red beds subgrade fillers. The merits of the research results including:

Received: 31 December 2020 Revised: 4 April 2021
This work was supported by the "13th Five-Year" National Key Research and Development Program of China(2016YFB1200401-102D).
First author: XU Hua, male, born in 1979, PhD, Associate Professor, mainly engaged in geotechnical and tunnel engineering research. E-mail: xuhua@swjtu.edu.cn

providing references for the design and construction of railways subgrade and other projects in the red bed area, and raising innovative methodology for studying the internal mechanism for the strength of soil-rock composite.

2 Compression test

2.1 Filler ratio

The Chengdu–Ya'an section of the Sichuan–Tibet Railway suffers heavy rainfall, with an average annual rainfall of 1,200–1,750 mm. Affected by the climate and environment, the red beds subgrade fillers have high moisture content and cannot be compacted during construction, and hence the improvement is necessary to obtain high quality fillers. At present, the research on the improvement of red beds subgrade fillers is mainly focusing on chemical methods[10–11], considered costly and causing negative effects on the ecological environment. In contrast, physical methods[12–13] that improve soil compaction characteristics by changing the gradation have the advantages of simple operation, lower cost and saving time. Therefore, for the construction of Chengdu–Ya'an section of the Sichuan–Tibet Railway, a physical improvement method via mixing red clay with certain proportion of weakly weathered mudstone rock is adopted for high-quality subgrade fillers.

In the borrow site of Mengdingshan Mixing Station in Ya'an, weakly weathered red-bed mudstone is selected and broken into rock fragments. The crushed stone admixture is made by mixing 3 particle sizes ranging from 5 to 10, 10 to 20 mm and 20 to 40 mm in a mass ratio of 1:2:1. This material has the characteristics of low weathering degree, hard texture, sharp-edged shape, and low moisture content. The mudstone rock in mass ratios of 40%, 50%, and 60% is mixed with the red-bed clay to obtain three types of improved red beds subgrade fillers numbered 1, 2, 3[14]. The uniformity coefficients of the improved red beds subgrade fillers were 20.5, 19.8, 15.8, and the curvature coefficients were 2.4, 2.9, 3.5, respectively. According to the *Code for design of railway earth structures* (TB10001-2016)[15], the three types of fillers were fine breccia with good grading, and subject to Group B fillers. Figure 1 shows the weakly weathered red-bed mudstone rock, and Figure 2 is the gradation curves for these improved red beds subgrade fillers.

Fig. 1 Weakly weathered red-mudstone fragments

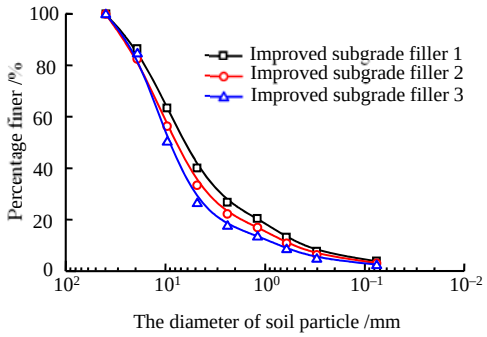

Fig. 2 Gradation curves of improved red beds subgrade fillers

2.2 Modified compaction test

The optimum moisture content and maximum dry density of the improved red beds subgrade fillers are the most important indicators to the compaction and settlement of the subgrade in field construction. According to the *Code for soil test of railway engineering* (TB10102-2010)[16], for the improved red beds subgrade fillers with maximum particle size 40 mm, the Z3 heavy-duty compactor was used for field compaction. The test adopted method of changing the moisture content of the intact soil so as to change the value for the improved fillers. The moisture content of the undisturbed soil was incrementally increased by 2.5%, and eventually controlled in the range of 15% to 25%. Figure 3 shows the compaction test curves of the improved red beds subgrade fillers composed of different proportions of rock fragment.

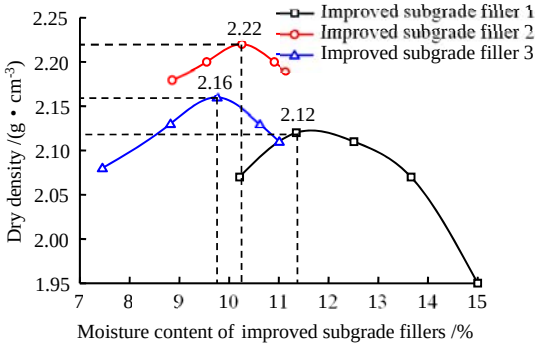

Fig. 3 Compaction curves of improved red beds subgrade fillers

The results of the field compaction test show that as the rock content increases, the optimum moisture content of the sample gradually decreases, and the red-bed mudstone crushed stone has a more obvious effect on reducing the moisture content of the undisturbed soil. The maximum dry density of modified fillers 1, 2 and 3 are 2.12, 2.22 and 2.16 g/cm^3, and the optimum moisture content are 11.24%, 10.26% and 9.76%. It indicates that the improved filler 2 has a larger maximum dry density.

2.3 Unconfined compression test

The laboratory unconfined compression test was carried out in accordance with the *Code for soil test of*

railway engineering (TB10102-2010)[16], using a micro-computer-controlled pressure testing machine (specification 1,000 kN, model WHY-1000). The loading was controlled at a rate of 3 mm/min. The samples were cylinders with a diameter of 152 mm and a height of 166 mm. In order to study the influence rule of gradation and moisture content on the strength of the fillers, the optimum moisture content and the dry side and wet side of the optimum moisture content were selected. For the compaction and particle uniformity of the sample, the sample was compacted in 3 layers, each layer was hit 94 times, and the degree of compaction was controlled above 95%. Table 1 shows the unconfined compressive strength values of different graded fillers under various moisture content conditions.

Table 1 The unconfined compressive strength

The species of fillers	Moisture content /%	Unconfined compressive strength /kPa
Improved subgrade filler 1	10.21	191.8
	11.24	108.0
	12.51	54.6
Improved subgrade filler 2	9.55	510.7
	10.26	421.9
	10.91	217.7
Improved subgrade filler 3	8.82	247.4
	9.76	219.1
	10.62	98.1

As shown in Table 1, the unconfined compressive strengths of the improved fillers 1, 2 and 3 are 108.0, 424.1 and 219.1 kPa when the moisture content is optimum. The moisture content has a significant effect on the unconfined compressive strength of the improved red beds subgrade fillers. The unconfined compressive strength gradually decreases with the increase of moisture content.

The influence of particle gradation has been studied. The improved fillers 1, 2 and 3 with moisture content of 10.21%, 10.26% and 10.62% were selected for analysis based on the rationale that the moisture content deviation was within 0.5%, thus major impact on the mechanical and deformation characteristics of fillers was avoided. Figure 4 shows the whole stress-strain curves of different improved fillers in the process of deformation and failure. The unconfined compressive strengths of the improved red beds subgrade fillers 1, 2 and 3 are 191.8, 421.9 and 98.1 kPa, respectively. The failure morphology of the samples shows different patterns of tensile failure (Fig. 5). Tensile cracks occurred in the samples, and the number, length and width of the cracks are obviously affected by the content of mixed rock. As the rock content increases, the frictional effect of the rock fragment becomes more significant. However, the decreasing soil content reduces the cohesion of the filler, and consequently the cracks tend to develop in the weak bonding position. For example, the vertical cracks in the improved red beds subgrade filler 3 shows faster evolution, the length and width of which are widely distributed as well. In contrast, the improved red beds subgrade filler 2 performs good integrity after failure. The sample has a tensile crack with a length of 124 mm and a width of 3 to 4 mm. Table 2 shows the crack statistics of the compression test of the improved red beds subgrade fillers.

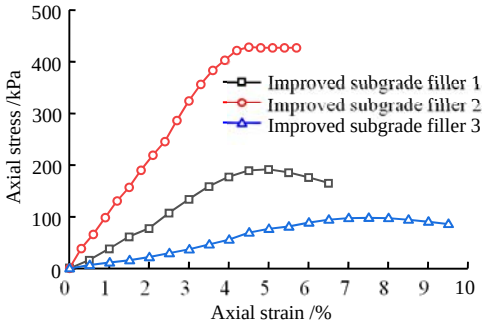

Fig. 4 Stress–strain curves of uniaxial compression test

(a) Filler 1 (b) Filler 2 (c) Filler 3

Fig. 5 The failure of samples

Table 2 The statistics of cracks in samples

Species	Number of cracks	Length /mm	Width /mm
Filler 1	3	26～52	2～3
Filler 2	1	124	3～4
Filler 3	5	24～70	3～6

The laboratory test shows that the content of rock fragment has a significant effect, in terms of macroscopic damage characteristics, on the mechanical properties of the improved red beds subgrade fillers. The PFC^{3D} numerical simulation software was used to simulate the whole process of the compression test, explaining the observed macro-mechanical phenomenon, and to study the internal mechanism of the impact of the rock fragments content on the mechanical properties of the improved red beds subgrade fillers.

3 Particle flow modelling of compression test

3.1 Geometric model for rock fragment

On the meso-scale, the shape of rock fragment is an important factor that affects the mechanical behavior and failure pattern of the composite soil[17]. Therefore, reproduction of the geometric model for the rock fragment is important for numerical study of the mechanical properties of the improved red beds subgrade fillers.

At present, the "random particle contour construction method" is dominantly implemented in the 3D geometric model reconstruction technology. Based on the basic geometry, the plane is randomly cut[18] or the

base point is randomly selected according to the algorithm of topological relationship to form an irregular polyhedron[19]. The methods are feasible for analysis. However, the geometric models are mostly convex polyhedron, and are obviously different from the concave and convex shape of the rock in field. To overcome this problem, the polyhedral structure method based on the ellipsoid surface was improved[7], and a geometric model of the rock with concave and convex polyhedron shape was proposed. The main principles and methods are as follows:

(1) Generate the base surface of the ellipsoid. The size and shape of the ellipsoid are determined by the three semi-major length parameters ($R_1 > R_2 > R_3$). Taking the half of the maximum size in the three-dimensional size of the actual rock particles as the R_1 parameter, the ratio of R_2 , R_3 to R_1 is equal to the ratio of the dimensions in the other two directions to the maximum dimension. In the actual situation, it is difficult to measure the three-dimensional size of the crushed stone particles sequentially. It is suggested to use the actual three-dimensional size characteristics of the crushed stone to determine the value range of R_1 , R_2 and R_3, and then construct a model that conforms to the actual statistical law.

(2) Select the base point of the ellipsoid base surface. In the Cartesian coordinate system, five parameters (R_1 , R_2 , R_3 , θ_i , φ_i) are needed to determine any point on the ellipsoid, the formulas of determining the random point coordinate parameters θ_i , φ_i are

$$\left.\begin{aligned}\theta_i &= \eta_1\pi \\ \varphi_i &= \frac{2\pi i}{N}\left[1+\delta(2\eta_2-1)\right];\ (i=1,\cdots,N)\end{aligned}\right\} \quad (1)$$

where N is the number of base points; η_1 and η_2 are uniformly distributed and independent random numbers in [0,1]; the value of variable δ is 0.3. The base point is expressed in a rectangular coordinate system as

$$\left.\begin{aligned}x_i &= R_1\sin\theta_i\cos\varphi_i \\ y_i &= R_2\sin\theta_i\sin\varphi_i \\ z_i &= R_3\cos\theta_i\end{aligned}\right\} \quad (2)$$

(3) Generate concave and convex surface. Randomly select m base points (x_i , y_i , z_i) to move to the center of the ellipsoid, the coordinate of the base point after the movement is $(x_i/a,\ y_i/a,\ z_i/a)$, the "a" is a random number greater than 1. The irregular concave-convex polyhedron is formed by algorithm connection, and then the geometric model of rock fragment conforming to the actual situation is reconstructed.

Use Matlab (2019 version) to get the geometry, and output ".stl", then import PFC3D to generate clump rock model. The geometric model of the rock fragment with the number of base points N being 10, 20, and 30 is displayed in Fig. 6.

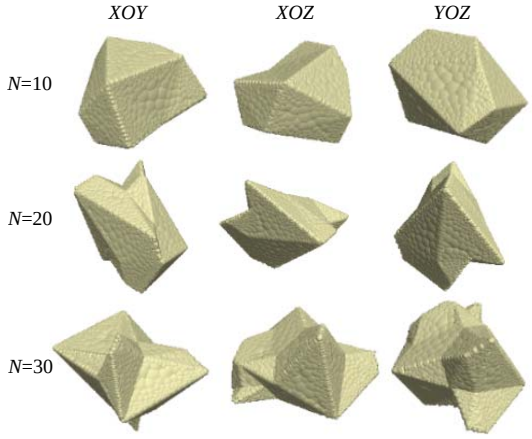

Fig. 6 The geometric model of red-mudstone fragments

This method can well construct a geometric numerical model for rock fragments with concavo-convex shapes. Constructed geometry of rock fragment conforms to the realistic fragment shape of weakly weathered red-bed mudstone (Fig. 1). Since the particles can produce frictional occlusion when the sample is loaded. Compared with the sample generated by a single sphere or convex polyhedron in PFC^{3D}[20], the peak strength and residual strength of the sample are enhanced.

3.2 Compression test particle flow model

The sieve test shows that the mass percentage of particle size less than 1.18 mm was 20% in the improved red beds subgrade fillers. Since the small particles have little effect on mechanism of composite subgrade fillers, the volume equivalent conversion algorithm[21] was adopted to convert the particles with the particle diameter less than 1.18 mm into normally distributed particles between 1 and 5 mm (which were generated according to the particle gradation using the "ball distribute" command) to improve the calculation efficiency. The value R_1 of the red-bed mudstone particle size is determined from the actual gradation of the improved red beds subgrade fillers, R_1 is between 5–40 mm. According to the statistics of the morphological characteristics of the red-bed mudstone rock, the length ratios of R_2 , R_3 to R_1 are within the ranges of 0.3–0.8 and 0.4–1.0, respectively. In this analysis, 26 geometric models of red mudstone rock were randomly generated. Utilizing servo control program for correction, the numerical simulation samples 1, 2, 3 of the improved red beds subgrade fillers were established (Fig. 7), and the total number of crushed stones was 958, 1194 and 1433, respectively.

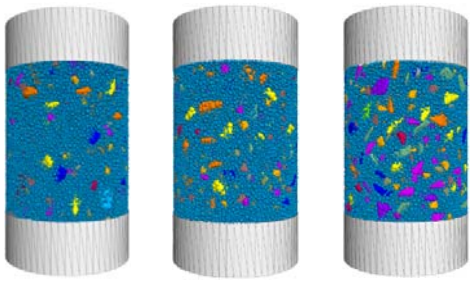

(a) Filler 1 (b) Filler 2 (c) Filler 3

Fig. 7 Numerical simulation model of improved red beds subgrade fillers under compression test

3.3 Meso-parameter calibration

The simulation of improved red beds subgrade fillers adopted the linear contact bond model, and the meso-parameters were given via the "contact method" and "cmat default" commands. The servo program was used to control the confining pressure as 0.2 kPa to simulate unconfined test as a special triaxial test with very small confining pressure. The program also prescribed the constant confining pressure and the speed of upper and lower loading plates at 0.001 m/s to compress the sample. The stress-strain changes were monitored.

As for determination of the meso-parameters of the model, it is concerned that the stiffness mismatch between the cohesive soil and the rock leads to continuous displacement and deformation inside the sample. Fissures are formed inside the soil and the rock fragments are not easy to be damaged during the deformation of the sample. Therefore, the soil and the gravel have a complex interaction relationship. In order to accurately study the physical and mechanical properties of the improved red beds subgrade fillers and the relationship between soil and rock, the parameters of soil and rock in the model cannot be simply set up to the identical values. Three different contact types are defined in the model: the contact between red-bed clay particles (soil–soil), the contact between clay particles and mudstone rock (soil–rock), and the contact between mudstone rocks (rock–rock). Different contact parameters are determined depending on the contact type. The viscous behavior between the red layer clay and the strong friction between the rock fragments can be simulated in the numerical analysis, realizing better reproduction of the complex soil-stone interaction for the improved red beds subgrade fillers. This simulation is also beneficial for analyzing the substantial mechanism of the impact of rock content on soil strength.

With reference to the relationship between meso-parameters and macro-mechanical phenomena proposed by Shi et al.[7], and the stress-strain curve of unconfined compression test, the trial and error method was used to determine the meso-parameters of three improved red beds subgrade fillers, as listed in Table 3. The numerical results are in good agreement with the stress-strain curve of the laboratory test. Figures 8(a) and 8(b) are the failure patterns of laboratory sample and numerical sample of the improved red beds subgrade filler 2. Figure 8(c) is the displacement angle distribution of the particles on the *XOZ* surface according to the regional statistics at the peak strength of the improved red beds subgrade filler 2. The angle refers to the angle between the normal direction of the particle displacement and the horizontal plane. In this figure, the main directions of particle displacement in all the four vertex areas tilt outward, instead of purely vertical downwards. The particles in the central area also mainly move to both sides. The results show that the sample is bulging and deformed as a entity, and tension cracks are formed inside, which is consistent with the failure pattern of the laboratory test.

Table 3 Numerical simulation parameters

Filler	Contact types	Elastic modulus /MPa	Stiffness ratio	Friction factor	Bond strength /kPa	
					Normal	Shear
1	soil–soil	8	1	0.4	440	880
	soil–rock	40	1	0.4	220	440
	rock–rock	80	1	0.7	0	0
2	soil–soil	12	1	0.7	760	1 520
	soil–rock	60	1	0.7	380	760
	rock–rock	120	1	1.1	0	0
3	soil–soil	1	1	0.6	150	300
	soil–rock	5	1	0.6	75	150
	rock–rock	10	1	1.1	0	0

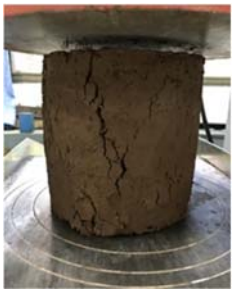

(a) Sample of indoor test

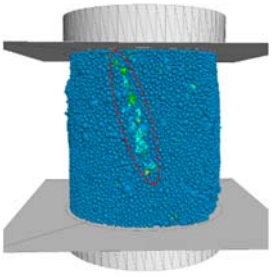

(b) Sample of numerical modelling

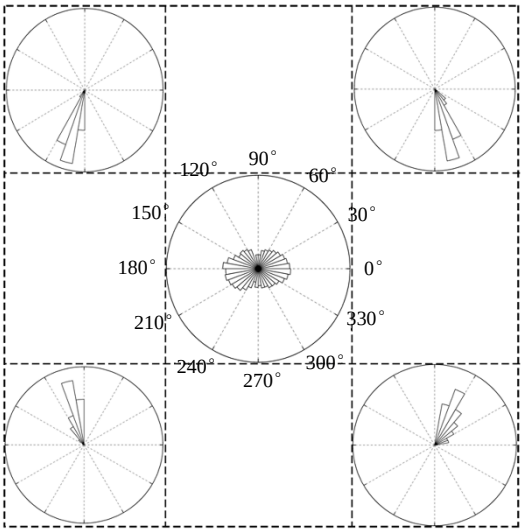

(c) Distribution of particle displacement angle

Fig. 8 The failure of specimen of improved red beds subgrade filling 2

4 Contact force chain

4.1 Spatial distribution of strong contact force chain

The study of granular material mechanics claims that the contact network in the system is the physical basis of the external load transfer path[22]. The research of this network system is basically to investigate the soil skeleton effect. The analysis of the evolution of the contact force chains including strong and weak force chains, aims at explaining the mechanism of the macro-mechanical behavior of the particle system. The strong contact force chain bears the main load and supports the entire system to resist deformation. Therefore, analyzing the evolution of the strong contact force chain is the focus of understanding the mechanical properties of the system.

The strain percentage parameter ξ (ξ = strain/peak strain × 100%) was introduced for comparative analysis. The contact force chain with the contact force F_c greater than the average value F and the contact angle θ_c greater than 45° was defined as a strong contact force chain[22–23]. Taking the improved red beds subgrade filler 2 as an example, the evolution of the internal force chain of the sample during different loading stages was analyzed. Figure 9 shows the spatial distribution of strong contact force chains at different strain stages. The green contact in the figure represents the strong force chain, whilst the blue one represents the weak force chain.

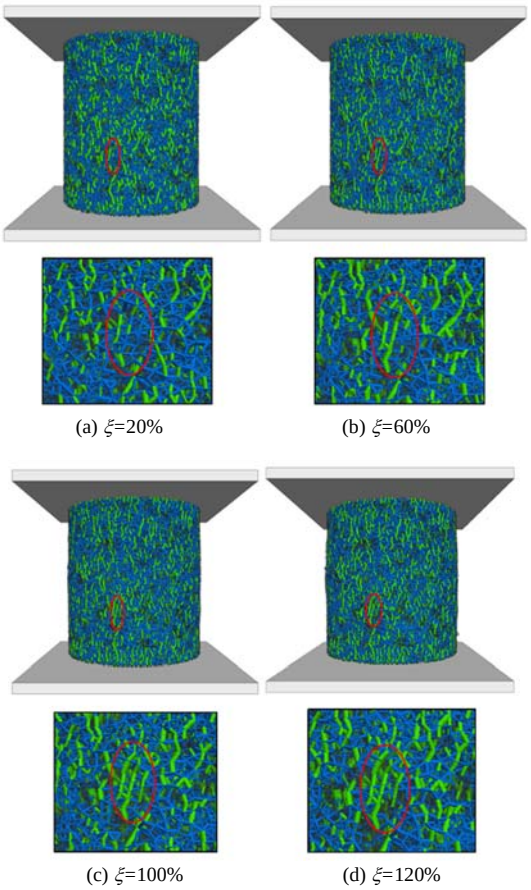

(a) ξ=20% (b) ξ=60%

(c) ξ=100% (d) ξ=120%

Fig. 9 Spatial distribution of strong force chains under different strains

It can be seen from the entire force chain network that the strong contact force chains are basically along vertical direction in space, forming long force chains to transmits vertical loads. The distributions of strong contact force chains performs large variance in different loading stages. The formation and disappearance of strong contact force chains in the system mainly depend on the stability of local structure. Taking the same position in the lower part of the sample (circled in red) as an example, at ξ = 20% (Fig 9(a)), the stress level in the system is low, and only a small part of the contacts forms strong contact force chains. With the increase of stress level, the force chains do not break even at the stage of ξ = 60%, 100%, and 120%, because some previously weak force chains transformed into strong force chains and the strong contact force chains structure are stable to bear the increase of system load. It reveals that the stronger occlusal friction effect, stable particle structure and small dislocation under loading lead to the basis for forming strong contact force chains in the system.

4.2 Dynamic change of strong contact force chain

To quantitatively present the evolution of strong contact force chains, the total number of strong contact force chains and the ratio of different type strong contact force chains to the total number of strong contact force chains in the system were shown in Figs. 10–12.

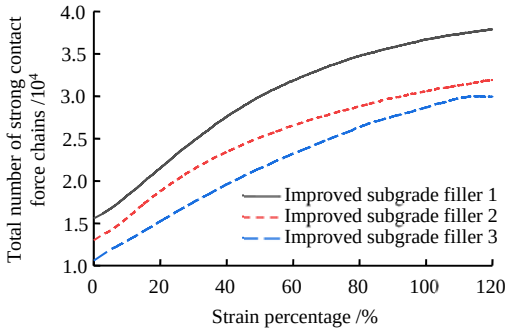

Fig. 10 The changes of strong force chain number

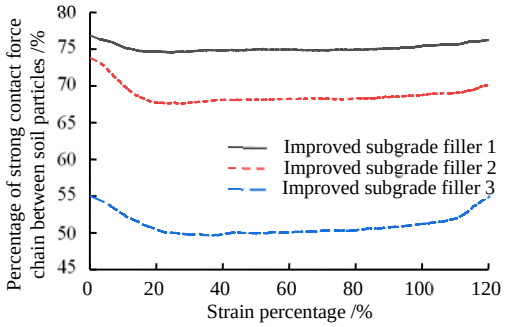

Fig. 11 The proportion of strong force chain number between soil particles

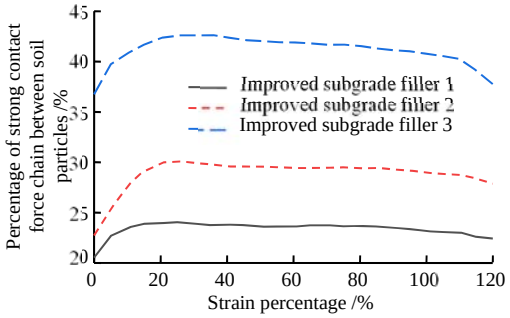

Fig. 12 The proportion of strong force chain number between soil and gravel

As seen in Fig.10, the total number of strong contact force chains gradually increases with the vertical pressure, and the trend slows down after the peak value. The higher rock content of the improved red beds subgrade fillers results in the reduction of total number of strong contact force chains in the system under the same strain percentage. The reason for this is that the total number of particles in the system decreases under

higher rock content, and consequently the contact frequency among particles decreases. As shown in Figs. 11 and 12, in the early stage of loading, the proportions of the strong contact force chains among soil particles all decrease rapidly by the amplitude of 2.4%, 6.2%, and 5.4% for improved red beds subgrade fillers 1,2, and 3. However, the corresponding data between the soil particles and the rock all behaves fast growing by the amplitudes of 3.5%, 7.4%, and 5.9%. It shows that the load-taking from the rocks is significant in the early stage of loading. The improved red beds subgrade filler 2 has a more uniform distribution of soil particles and rock fragments, and has a good force chain network which provides a structural basis for the most stress transmission chains. As the loading process continues, due to the small bonding strength between soil particles and rock, the contact breaks first and then it leads to a decrease in the proportion of strong contact force chains between soil particles and rock. The increase in the proportion of strong contact force chains between soil particles is observed.

4.3 Magnitude distribution of strong contact force chain

The load-sharing relationship of force chains during the loading process is analyzed utilizing dynamic changes of different types of strong contact force chains as described in section 3.2. However, the distribution of contact force values of different types of strong contact force chains in the system is unknown yet. The current research mainly analyzes the distribution rule of the overall contact force chain of the sample[24–25], but the mechanism of different types of contact force chains on the strength of the soil–rock composite cannot be clarified based on the overall analysis. To solve this problem, the value of the strong contact force chain is normalized into a dimensionless quantity f. Take the strong contact force chain between soil particles and rock as an example:

$$f_{\mathrm{sr}}=\frac{F_{\mathrm{sr}}}{\sum F / N_{\mathrm{p}}} \tag{3}$$

where the subscript sr (soft–rock) represents the contact between the soil particles and the rock; F_{sr} is the value of a strong contact force chain between the soil particle and the rock; $\sum F$ represents the total value of all strong contact force chains in the system; and N_{p} is the total number of strong contact force chains in the system. The strong contact force chains between soil particles and soil particles and between rock and rock can be normalized as f_{ss} and f_{rr} in the same fashion.

The normalized f_{sr} is divided into 12 equal intervals of 0.5 and the total interval value is 6.0. The number of f_{sr} in each interval is counted to obtain the probability density:

$$P(f_{\mathrm{sr}})=\frac{M_{\mathrm{sr}}}{N_{\mathrm{sr}}} \tag{4}$$

where M_{sr} is the total number of f_{sr} in a certain interval; N_{sr} is the total number of strong contact force chains between soil particles and rock. The probability density ($P(f_{\mathrm{ss}})$, $P(f_{\mathrm{rr}})$) of the other two contact types can be obtained using the same method.

According to the statistical analysis steps, the probability density distribution curves (Fig. 13) of different types of strong contact force chains at the peak strength of the sample were obtained. It is found that the distribution manner of different types of strong contact force chains is obviously different with the change of rock content. But a general trend of first increases and then decreases is followed, and the probability density is the maximum in the interval of 0.5 to 1.0.

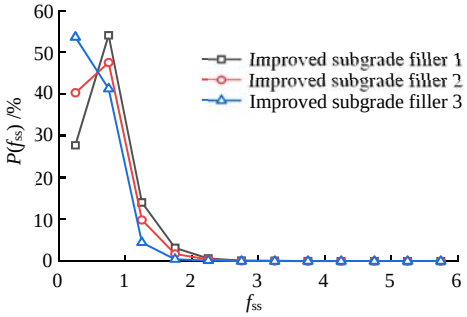

(a) Probability distribution curves of strong contact force chains between soils

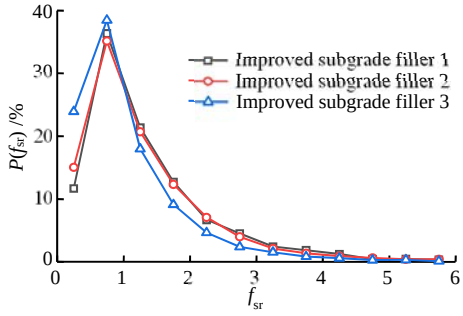

(b) Probability distribution curves of strong contact force chains between soil and rock

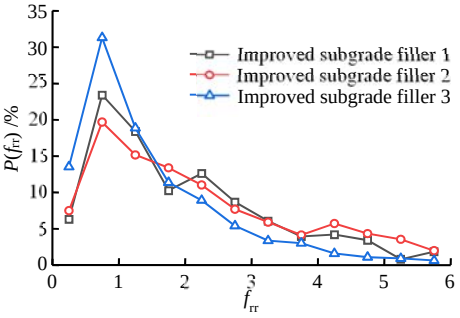

(c) Probability distribution curves of strong contact force chains between rock and rock

Fig. 13 Probability density distribution of different strong force chain at peak strength

In Figure 13(a), the distribution manner of the strong contact force chains of the improved red beds subgrade filler decreases in an exponential trend as the rock content increases. For the sample of high rock content, it is difficult for soil particles to completely fill the pores due to large porosity in the system. As a result,

the f_{ss} distribution is generally reduced, which is consistent with the probability density of strong contact force distribution of biaxial compression in Zhang et al.[25]. In Fig. 13(b), the similar probability distributions of the improved red beds subgrade filler 1 and 2 are revealed. For the improved red beds subgrade filler 3, the probability value is lower than those of the fillers 1 and 2 when $f_{sr} > 1.0$, but it is greater than filler 1 and 2 when $f_{sr} < 1.0$. In Fig.13(c), the distribution probabilities of strong contact force chains of the improved red beds subgrade for fillers 1, 2, and 3 are 66%, 70%, and 44%, respectively when $f_{rr} > 1.0$. Specifically, when $f_{rr} > 3.5$, this index for strong contact force chains of the improved red beds subgrade filler 2 is obviously greater than that of the other two. Referring to the compression test results, it is concluded that the clay and rock fragments in filler 2 (rock content is 50%) construct good contact and thus develop clay bondage and super-strength chains. The sample has a better particle framework supporting system to bear the load, so the improved red beds subgrade filler 2 has the highest strength. The probability density of the improved red beds subgrade filler 3 is lower than the other two for $2.0 < f_{rr} < 6.0$, although the rock content is 60%. As for the smaller unconfined compressive strength of the improved red beds subgrade filler 3, it is for the reason that the occlusal effect of the rock fragments is weaker due to the lack of filling auxiliary effect of anisotropic weak force chains and it leads to a worse ability to generate super-strength chains. Figure 14 is a simplified diagram of the distribution of soil particles and rock in the unconfined compression test, which can intuitively explain this mechanism.

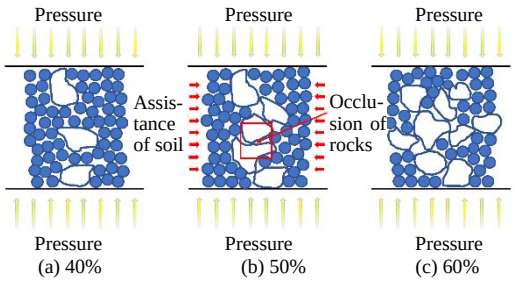

Fig. 14 Distribution of soil and gravel under uniaxial compression test with different rock contents

The dimensionless quantity f is a useful index for different types of strong contact force chains. The comparison of probability density distribution of different types of strong contact force chains in the system is helpful to understand the internal mechanism of bearing capacity development in the composite sample. The probability density distribution is further quantitatively analyzed to characterize the degree of influence of different types of strong contact force chains on the bearing capacity.

The improved red beds subgrade filler 1 is taken as an example. Based on the results of $P(f_{ss})$, $P(f_{sr})$ and $P(f_{rr})$, the following approach is used for quantitative analysis:

Take the midpoint f' of each interval in the probability density distribution diagram as the row vector $\boldsymbol{x}$:

$$x = [0.25,\ 0.75,\ 1.25,\ 1.75,\ 2.25,\ 2.75,\ 3.25,\ 3.75,\ 4.25,\ 4.75,\ 5.25,\ 5.75] \tag{5}$$

A matrix with $P(f_{ss})$, $P(f_{sr})$ and $P(f_{rr})$ is formed:

$$\Delta_1 = [\alpha^1_{P(f_{ss})},\ \beta^1_{P(f_{sr})},\ \gamma^1_{P(f_{rr})}] \tag{6}$$

where the subscript 1 of the matrix and the superscript 1 of the vector represent the improved red beds subgrade filler 1.

For the convenience of analysis, the strength converted value q is derived with firstly multiplying the midpoint of each interval with the corresponding distribution value for a contact type, and then adding up. Take the contact between soil particles and rock as an example:

$$q^1_{sr} = x \cdot \beta^1_{P(f_{sr})} \tag{7}$$

Then the strength converted values of 3 different contact types are obtained as

$$\delta_1 = [q^1_{ss},\ q^1_{sr},\ q^1_{rr}] = x \cdot \Delta_1 = [x\alpha^1_{P(f_{ss})},\ x\beta^1_{P(f_{sr})},\ x\gamma^1_{P(f_{rr})}] \tag{8}$$

Add the strength converted values of the three different contact types to obtain the strength converted value Q_1 of the improved red beds subgrade filler 1:

$$Q_1 = q^1_{ss} + q^1_{sr} + q^1_{rr} \tag{9}$$

Therefore, the converted strength values of the improved red beds subgrade fillers 1, 2, and 3 can be obtained (Table 4) following the approach above.

Table 4 The strength converted values

Species	q_{ss}	q_{sr}	q_{rr}	Q
Filler 1	0.730	1.328	1.958	4.016
Filler 2	0.624	1.273	2.144	4.041
Filler 3	0.511	1.039	1.478	3.028

As shown in Table 4, the converted strength value of the improved red beds subgrade fillers 1, 2, and 3 are 4.016, 4.041, and 3.028, respectively. The larger the strength converted value, the better the mechanical properties of the improved red beds subgrade fillers. Therefore, the mechanical properties of the improved red beds subgrade fillers with rock content are in the order of 50%>40%>60%, and the results are consistent with the data from laboratory compression test. In these results, the q_{rr} of the improved red beds subgrade filler 2 reached 2.144, which contributed 53.1% to the overall strength converted value of 4.041, while the corresponding data of the other two fillers was 48.8%. It indicates that when the rock content is 50%, the load bearing effect of the strong contact force chains between the rocks is enhanced, and the friction effect of the rocks is the optimistic incorporating clay filling. Com-

pared with the other two materials, the rigidity and high strength of rock fragments are well developed. Therefore, for the design of improvement for red clay roadbed, it is recommended that a 50% content of weakly weathered mudstone rock fragments is mixed with the red bed soil.

5 Conclusion

The study focused on the macro mechanical properties of the improved red beds subgrade fillers of the Sichuan–Tibet railway and the meso mechanism of the strong contact force chains through laboratory compression test and PFC numerical simulation to explain the substantial mechanism affecting the strength of the fillers. The main conclusions are as follows:

(1) The characteristics of strength and deformation of the improved subgrade fillers are significantly affected by the content of mixed rock. Tests have shown that the incorporating of more red-bed mudstone rock has a more significant effect on reducing the optimal moisture content of improved subgrade fillers. The unconfined compressive strength of improved subgrade fillers gradually decreases as water content exceeds the optimum water content. Among the three samples, the improved red beds subgrade filler 2 which contains 50% of weathered stone realizes better strength and deformation characteristics.

(2) An approach for modelling rock geometry with concave-convex polyhedron shape randomly is proposed. It accurately reflects the actual rock shape and simulate the effect of real rock particles for better investigation of the micromechanical properties of soil–rock mixtures.

(3) As the improved red beds subgrade filler is loaded, the proportion of the strong contact force chain between the soil particles and the rock increases rapidly, while the corresponding value between soil particles and soil particles decreases rapidly. It reveals an obvious stress transfer effect between the soil–soil contact and the soil–rock contact in the system. The rock fragments play an important role in bearing the load.

(4) A new perspective is proposed to quantify the proportion of different types of strong contact force chains for different improved subgrade fillers. The internal mechanism of the strength change of the modified filler can also be explained by analyzing the distribution rule of different types of strong contact force chains. It shows that when the rock content is 50%, the strong contact force chains between the rocks is better than the other samples because the appropriate proportion of clay particles play the role of filling and bonding for the system, and thus an effective super-strength chain among the rock fragments is formed.

(5) This study has proven that the red beds subgrade filler with 50% of weathered stone added has greater strength, better effects of occluding and extrusion between rocks, and suitable soil and rock structure for strong contact force chains development. For the engineering design of red clay roadbed, it is recommended that the proportion of weakly weathered mudstone rock fragment for the improved fill is 50%.

References

[1] FENG Qiang. Study on the distribution and pavement performance of red bed mudstone in Sichuan province[D]. Chengdu: Southwest Jiaotong University, 2011.

[2] JU Neng-pan, HUANG Hai-feng, ZHENG Da, et al. Improved Burgers model for creep characteristics of red bed mudstone considering water content[J]. Rock and Soil Mechanics, 2016, 37(Suppl.2): 67–74.

[3] XU Hua, ZHANG Yi-bo, ZHANG Jie, et al. Experimental research on the mechanical properties of improved red soil subgrade in rich water area[J]. Journal of Railway Engineering Society, 2017, 34(11): 9–13.

[4] XU Hua, MOVAHED MA, YOU Guan-jun, et al. Experiment and compaction technology study on improved filler of red mudstone in Sichuan-Tibet railway[J]. Railway Construction Technology, 2019(10): 12–17.

[5] WANG Xu-yi, HUANG Shu-ling, DING Xiu-li, et al. Study on the effect of inhomogeneous bedding plane on the mechanical properties of uniaxial compression of layered rock mass[J]. Rock and Soil Mechanics, 2021, 42(2): 581–592.

[6] ZHU Yan-bo, YU Hong-ming, YANG Yan-xia, et al. Indoor experimental research on characteristics of improved red-mudstone[J]. Chinese Journal of Rock Mechanics and Engineering, 2013, 32(2): 425–432.

[7] SHI Chong, ZHANG Qiang, WANG Sheng-nian. Numerical simulation technology and application with particle flow code(PFC5.0)[M]. Beijing: China Architecture & Building Press, 2018.

[8] ZHOU Jian, WANG Jia-quan, ZENG Yuan, et al. Slope safety factor by methods of particle flow code strength reduction and gravity increase[J]. Rock and Soil Mechanics, 2009, 30(6): 1549–1554.

[9] CONG Yi, CONG Yu, ZHANG Li-ming, et al. 3D particle flow simulation of loading-unloading failure process of marble[J]. Rock and Soil Mechanics, 2019, 40(3): 1179–1186.

[10] ZHANG Zhong-yun, JIANG Guan-lu, WANG Zhi-meng. Experimental study on the physical and mechanical properties of red bed mudstone modified soil filler[J]. Sichuan Architecture, 2008, 28(1): 101–102.

[11] XU Peng, JIANG Guan-lu, REN Shi-jie, et al. Experimental study of dynamic response of subgrade with red mudstone and improved red mudstone[J]. Rock and Soil Mechanics, 2019, 40(2): 678–683.

[12] SHI Xiong, ZHANG Jia-sheng, LIU Bei, et al. Test of high-speed railway coarse grained filler of improved particle size distribution[J]. Journal of Central South University (Science and Technology), 2014, 45(11): 3964–3969.

[13] YANG Jun, YUAN Kai, DI Xian-jun, et al. Experiment and mathematical model on mechanical properties of natural gravel improving expansive soil[J]. Journal of Jiangsu University (Natural Science Edition), 2016, 37(3): 359–366.

[14] ZHANG Jie. Study on mechanical properties and deformation prediction of coarse particle modified filler in red bed of Sichuan-Tibet Railway[D]. Chengdu: Southwest Jiaotong University, 2019.

[15] China Railway First Survey and Design Institute Group Co. Ltd. TB10001－2016 Code for design of railway earth structure[S]. Beijing: China Railway Publishing House, 2017.

[16] China Railway First Survey and Design Institute Group Co. Ltd. TB10102－2010 Code for soil test of railway engineering[S]. Beijing: China Railway Publishing House, 2011.

[17] CHO G C, DODDS J, SANTAMARINA J C. Particle shape effects on packing density, stiffness, and strength: natural and crushed sands[J]. Journal of Geotechnical and Geoenvironmental Engineering, 2006, 132(5): 591–602.

[18] NASSAUER B, LIEDKE T, KUNA, M. Polyhedral particles for the discrete element method[J]. Granular Matter, 2013, 15(1): 85–93.

[19] TIAN Hu-nan, JIAO Yu-yong, WANG Hao, et al. Research on biaxial test of mechanical characteristics on soil-rock aggregate (SRA) based on particle flow code simulation[J]. Chinese Journal of Rock Mechanics and Engineering, 2015, 24(Suppl.1): 3564–3573.

[20] JIN Lei, ZENG Ya-wu, LI Jing-jing. Analysis on meso-mechanisms of influence of rock block shape on mechanical properties of cemented soil-rock mixture[J]. Acta Mechnica Solida Sinica, 2015, 36(6): 506–516.

[21] ZHANG Zhi-hua. Numerical simulation of coarse grained soil triaxial test based on PFC^{3D}[D]. Yichang: China Three Gorges University, 2015.

[22] SUN Qi-cheng, XIN Hai-li, LIU Jian-guo, et al. Skeleton and force chain network in static granular material[J]. Rock and Soil Mechanics, 2009, 30(Suppl.1): 83–87.

[23] PETERS J F, MUTHUSWAMY M, WIBOWO J, et al. Characterization of force chains in granular material[J]. Physical Review E Statistical Nonlinear & Soft Matter Physics 2005, 72(4): 041307.

[24] CHANG Ming-feng, PEI Jian-zhong, HUANG Ping-ming, et al. Analysis on the distribution probability of force chain of contact force among granular matter considering gradation[J]. Materials Review, 2018, 32(20): 3618–3622.

[25] ZHANG Wei, ZHOU Jian, YU Shi-wei, et al. Investigation on contact force and force chain of granular matter in biaxial compression[J]. Chinese Journal of Applied Mechanics, 2018, 35(3): 530–537.